

High-pressure phase transitions and melt structure of PbO₂: An analog for silicaBora Kalkan ^{1,2,*}, B. K. Godwal,³ Jinyuan Yan ² and Raymond Jeanloz^{3,4}¹*Earth and Planetary Sciences Department, University of California, Santa Cruz, California 95064, USA*²*Advanced Light Source, Lawrence Berkeley National Laboratory, Berkeley, California 94720, USA*³*Department Earth and Planetary Science, University of California, Berkeley, California, USA*⁴*Department Astronomy and Miller Institute for Basic Research in Science, University of California, Berkeley, California, USA*

(Received 14 September 2021; revised 11 February 2022; accepted 15 February 2022; published 25 February 2022)

In situ x-ray diffraction measurements and inverse Monte Carlo simulations of pair distribution functions were used to study the structural response of PbO₂ under pressure and to characterize the local structure of liquid PbO₂. Two phase transitions are observed upon room-temperature compression of crystalline PbO₂ up to ~65 GPa. The starting mixture of rutile structured β -PbO₂ and orthorhombic α -PbO₂ undergoes a transition to a ZrO₂-type orthorhombic phase with space group *Pbca* at ~21 GPa. Above 42 GPa, the *Pbca* phase transforms to a cotunnite-type phase with space group *Pnam*. In this paper, we also report short-range order in liquid PbO₂, showing ~8–9-fold and 4–5-fold coordination around Pb and O atoms, respectively.

DOI: [10.1103/PhysRevB.105.064111](https://doi.org/10.1103/PhysRevB.105.064111)**I. INTRODUCTION**

Silica (SiO₂) is a major constituent of planetary interiors. At ambient pressure, crystalline silica includes the quartz and its polymorphs: cristobalite and tridymite [1]. Thereafter, α -quartz shows a series of structural phase transitions with increasing pressure: quartz \rightarrow coesite \rightarrow stishovite \rightarrow CaCl₂ type \rightarrow α -PbO₂ \rightarrow pyrite type (268 GPa, 1800 K) [2–4]. Post-pyrite-type structures are identified using first-principles calculations [5–8]. At low temperatures, the transition from pyrite to Fe₂P type is expected to occur at ~750 GPa. Above 1000 K, silica first transforms from the pyrite-type structure to cotunnite and then to Fe₂P type [9]. Lyle *et al.* [10] recently predicted silica to transform from the 9-coordinated Fe₂P polymorph to a 10-coordinated tetragonal structure (*I4/mmm*) with concomitant metallization ~10 TPa.

Analogous to SiO₂ such as TiO₂, GeO₂, and SnO₂ have been studied extensively, the interest being to experimentally document the high-pressure phases of SiO₂ at relatively low pressures. At ambient conditions, rutile is the most stable phase of TiO₂, and it undergoes a sequence of phase transitions with pressure: rutile \rightarrow α -PbO₂ type \rightarrow orthorhombic-I \rightarrow orthorhombic-II (related to pyrite type) \rightarrow cotunnite type (>50 GPa) \rightarrow Fe₂P type (210 GPa, 4000 K) [11–13]. It is also predicted to transform from the Fe₂P type to the tetragonal phase (*I4/mmm*) ~6.5 Mbar [10,14]. GeO₂ occurs in α -quartz and rutile structures at ambient conditions, with several high-pressure transitions: α -quartz \rightarrow *P2₁/c* \rightarrow rutile \rightarrow CaCl₂ \rightarrow α -PbO₂ \rightarrow pyrite type [2,15–17]. *Ab initio* calculations predict the sequence: rutile \rightarrow CaCl₂ \rightarrow α -PbO₂ \rightarrow pyritetype \rightarrow cotunnite (300 GPa) \rightarrow Fe₂P [13,18]. Haines and Leger [19] studied SnO₂ up to 49 GPa using nonhydrostatic pressure media (grease and

16:3:1 methanol-ethanol-water mixtures), observing the structural transitions: rutile \rightarrow CaCl₂ \rightarrow α -PbO₂ \rightarrow pyrite type. This is like the high-pressure sequence found for GeO₂, the difference lying in the transition pressures. For example, the pyrite phase of GeO₂ occurs in the range 70–90 GPa [2,20] compared with SnO₂ for which it is observed ~49 GPa. Using x-ray diffraction at high pressures and temperatures with argon as pressure medium, Shieh *et al.* [21] observed a rutile \rightarrow CaCl₂ \rightarrow pyrite \rightarrow ZrO₂ \rightarrow cotunnite structural sequence in SnO₂. The ZrO₂ (*Pbca*) phase is found between 50 and 74 GPa under room-temperature compression, and the cotunnite phase observed at 54–117 GPa when laser heated between 1200 and 1500 K and then quenched.

Lead oxide (PbO₂) is another promising analog for SiO₂. Two forms of lead oxide are found as minerals on Earth's surface: orthorhombic α -PbO₂ (scrutinyite) and tetragonal rutile structured β -PbO₂ (plattnerite) [4]. Using x-ray diffraction with a nonhydrostatic pressure medium (grease), Haines *et al.* [16] and Haines and Leger [19] observed the sequence of transitions in β -PbO₂: rutile \rightarrow (4 GPa) CaCl₂ \rightarrow (7 GPa) *Pa-3* \rightarrow (11.4 GPa) *Pbca* \rightarrow (>29 GPa) cotunnite. The α -PbO₂ form also adopted the pyrite phase at 7 GPa and showed the coexistence of *Pbca* and *Pnam* phases from 29 to 47 GPa. Grocholski *et al.* [4] studied PbO₂ polymorphs up to 140 GPa in a laser-heated diamond-anvil cell under more hydrostatic conditions, with argon as a pressure medium. They applied laser heating to avoid the multiphase mixtures formed in the experiments of Haines and Leger [19] at room temperature. Further, they observed the baddeleyite-type structure in room-temperature compression measurements, which was absent from the results of Haines and Leger [19]. It is also to be noted that, in PbO₂, the cotunnite phase is observed at low pressures (24 GPa) using laser heating [4] as compared with SnO₂ for which it occurs at 54 GPa [19], suggesting that PbO₂ is the better analog for

*bkalkan@ucsc.edu

silica. The baddeleyite phase that was observed by Grocholski *et al.* [4] in the 30–40 GPa range was absent from the data of Haines and Leger [19]. In the study by Grocholski *et al.* [4], laser heating of β -PbO₂ succeeded in preventing the mixed-phase region [*Pbca* (OI) and cotunnite (*Pnam*) from 29 to 47 GPa] in the studies of Haines and Leger [19], and a pure cotunnite phase was documented. The main difference between their studies was the degree of deviatoric stress and strain achieved through laser heating and use of different pressure media. We carried out our study with neon as a pressure medium to check the sensitivity of the phase-transition pressures on deviatoric stress and strain.

In addition, we carried out high-pressure x-ray diffraction measurements to study the structure of liquid PbO₂, the closest analog to liquid SiO₂ at ultrahigh pressures as compared with SnO₂, GeO₂, and TiO₂: liquid PbO₂ is expected to become metallic at low pressures. At ambient conditions, PbO₂ melts at 365 K compared with other analogs which melt at high temperatures and show similar structural changes at low pressures as (nonmetallic) silica. Thus, studies on melt structure at moderate pressures are important for understanding metallic silica at extreme conditions. The melting temperature and melt-structure properties of analog materials more generally provide important insights into silica phases at extreme pressure-temperature conditions [22]. The laboratory data in fact provide benchmarks for first-principles density functional-based molecular dynamics simulations representing the current means of exploring the properties of giant planetary interiors [23]. These high-pressure results on fluids are of interest because melting is the main process by which the interiors of terrestrial planets evolve, and melting phenomena and melt structure are of widespread importance in physical sciences.

II. METHODS

Polycrystalline PbO₂ (Sigma Aldrich >99% purity) was ground into micron-sized grains and loaded into a symmetric diamond cell and a BX-90 diamond-anvil cell equipped with a tungsten resistive heater; these are driven by a gas membrane for the room-temperature–high-pressure and high-temperature–high-pressure experiments, respectively. Type Ia diamonds with 200- μ m-diameter culets were mounted on tungsten carbide seats on the upstream side of each cell. We used BN backing plates with opening angles on the detector side that allowed diffraction data to be collected up to maximum scattering vector magnitude $Q = 7 \text{ \AA}^{-1}$, corresponding to a resolution in radial distribution functions (RDFs) $\Delta r \sim 0.89(\pm 0.04) \text{ \AA}$. Sample chambers were formed by drilling holes with a diameter of 80 μ m in Re foil that was pre-indented to 30 μ m thickness. Liquefied neon served as the pressure-transmitting medium in compression experiments. Ruby spheres of $\leq 5 \mu$ m diameter were placed inside the sample chamber, and the ruby fluorescence technique was used to determine the pressure [24]. Online ruby (Al₂O₃ : Cr³⁺) fluorescence was used to determine pressure of the hot sample. Temperature was measured to an accuracy of ± 5 K up to 900 K using a K-type thermocouple next to the diamond culet [25].

Angle-dispersive x-ray diffraction experiments were performed at beamline 12.2.2 at the Lawrence Berkeley National Laboratory Advanced Light Source [26]. A monochromatic x-ray beam with $\lambda = 0.4959 \text{ \AA}$ (25 keV) was focused to an approximate size of $10 \times 10 \mu\text{m}$. Diffracted x rays were collected by a Mar345 detector at a distance of $331.4 \pm 0.1 \text{ mm}$. Detector distance and orientation were calibrated using a LaB₆ standard. The diffraction images were radially integrated using the programs FIT2D [27] and DIOPTAS [28]. The CELREF program [29] was used to refine unit cell parameters. To determine the structural parameters, the diffraction patterns were analyzed by performing Rietveld refinements using the GSAS software [30].

For room-temperature–high-pressure experiments, the sample was pressurized upon compression with 1–3 and 3–6 GPa steps in the pressure ranges of $P < 32 \text{ GPa}$ and $P > 32 \text{ GPa}$, respectively. In the case of high-temperature–high-pressure measurements, the sample was taken to the desired pressure first and then put through a heating and cooling cycle. We observed consistent pressure shifts during each cycle, caused by thermal expansion of the diamond-cell components; these were compensated with gas-driven pressure. Complete melting of PbO₂ is identified by loss of long-range order, indicated by the disappearance of x-ray diffraction peaks of the crystalline phase and a simultaneous increase in diffuse scattering over the entire 2θ range.

The technique used to obtain partial structure factors (PSFs) and to derive structural models of liquid PbO₂ was the empirical potential structure refinement (EPSR) method [31]. A Monte Carlo computer simulation of the system PbO₂ was created using 1000 Pb and 2000 O atoms within a cubic box. Atoms interacted via a Lennard-Jones (12-6) potential and Coulomb term [32]. The parameters defining the interatomic pair potentials used in the structure refinements, taken from Ref. [33,34], are as follows for O and Pb :

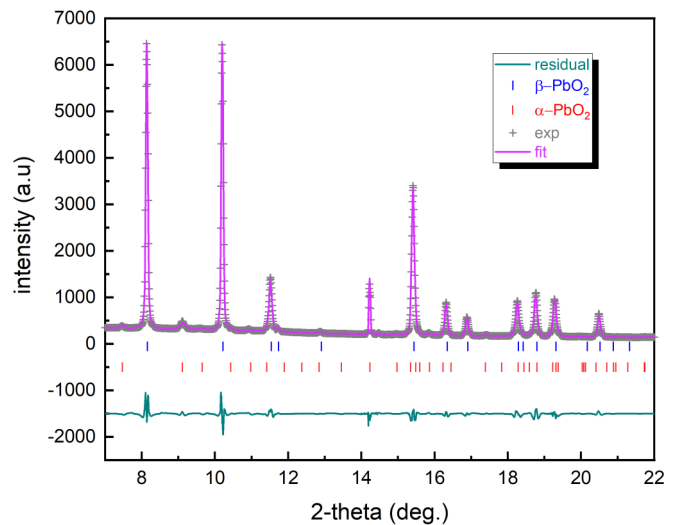


FIG. 1. X-ray diffraction pattern of PbO₂ at ambient conditions and the corresponding multiphase Rietveld refinement. The plus symbols and red lines are observed and calculated patterns, respectively, and vertical bars denote allowed Bragg reflections for PbO₂ polymorphs. The bottom trace (green line) shows the difference between the observed and calculated patterns.

TABLE I. Wyckoff positions of the phases of PbO₂.

Phase	Space group	Mineral name, structure type	Z	Atomic parameters
1	$P4_2/mnm$	β -PbO ₂ , rutile type, plattnerite	2	Pb 2a (0,0,0) O 4f (0.3066, 0.3066, 0)
2	$Pbcn$	α -PbO ₂ , scrutinyite	4	Pb 4c (0, 0.1779, 0.250) O 8d (0.2685, 0.4010, 0.4248)
3	$Pbca$	ZrO ₂ type	8	Pb 8c (0.8861, 0.02504, 0.2638) O 8c (0.7963, 0.3800, 0.1381) O 8c (0.9777, 0.7500, 0.4901)
4	$Pnam$	Cotunnite type	4	Pb 4c (0.260, 0.100, 0.250) O 4c (0.360, 0.430, 0.250) O 4c (0.020, 0.340, 0.750)

$\varepsilon_O = 0.1625 \text{ kJ mol}^{-1}$, $\sigma_O = 3.6 \text{ \AA}$, $q_O = -2e$, and $\varepsilon_{Pb} = 0.20 \text{ kJ mol}^{-1}$, $\sigma_{Pb} = 2.40 \text{ \AA}$, $q_{Pb} = 4e$. The edge lengths of the simulation cubic box with periodic boundary conditions for liquid PbO₂ are 37.11 and 36.84 Å, derived from the atomic number densities of 0.0587 atoms/Å³ (at 901 K/4 GPa) and 0.0600 atoms/Å³ (at 773 K/8 GPa) [35]. In addition, minimum distances of approach were set at: 1.24 Å (Pb-Pb), 1.73 Å (Pb-O), and 2.21 Å (O-O) [32,33]. A starting model was obtained by successive iterations (convergence in ~ 1200 iterations) of the system under the reference potential at 901 and 773 K. Structural parameters and their distributions reported here were obtained over many configurations (> 15000 iterations) of the models as they fluctuate about the final equilibrium energy, at which the structure factors of the model and experiment are in good agreement.

III. RESULTS AND DISCUSSIONS

X-ray diffraction results shown in Fig. 1 confirm that the starting material was rutile structured β -PbO₂ ($P4_2/mnm$, $Z = 2$) with a small contribution of naturally occurring orthorhombic α -PbO₂ ($Pbcn$, $Z = 4$). Rietveld refinement of the

structure yielded lattice parameters $a = b = 4.9342(2) \text{ \AA}$, $c = 3.3736(2) \text{ \AA}$, and $a = 4.9850(9) \text{ \AA}$, $b = 5.8946(9) \text{ \AA}$, $c = 5.4538(8) \text{ \AA}$ for β -PbO₂ and α -PbO₂, respectively. The starting values for Pb and O atomic coordinates for the observed phases are listed in Table I.

A. Compression at room temperature

Figure 2(a) shows the room temperature x-ray diffraction patterns for PbO₂ collected upon compression in the pressure range of 1.3–60 GPa. At pressures ~ 13.6 GPa, the intensities of the diffraction peaks for the β -PbO₂ and α -PbO₂ phases start to decrease, and these phases almost completely disappear at ~ 24.5 GPa. Bragg peaks for a new crystalline phase start to grow at 15.8 GPa, but β -PbO₂ and α -PbO₂ phases remain present. The new crystalline phase can be indexed as orthorhombic (space group $Pbca$, No. 61) with unit cell dimensions $a = 10.2011(96) \text{ \AA}$, $b = 5.2540(52) \text{ \AA}$, and $c = 5.1450(63) \text{ \AA}$ at 24.5 GPa, and it remains stable up to 39.3 GPa. The most intense peak of the orthorhombic phase (at $\sim 9.8^\circ 2\theta$) starts to disappear at 43.3 GPa, and new peaks appear. The diffraction pattern of this high-pressure phase

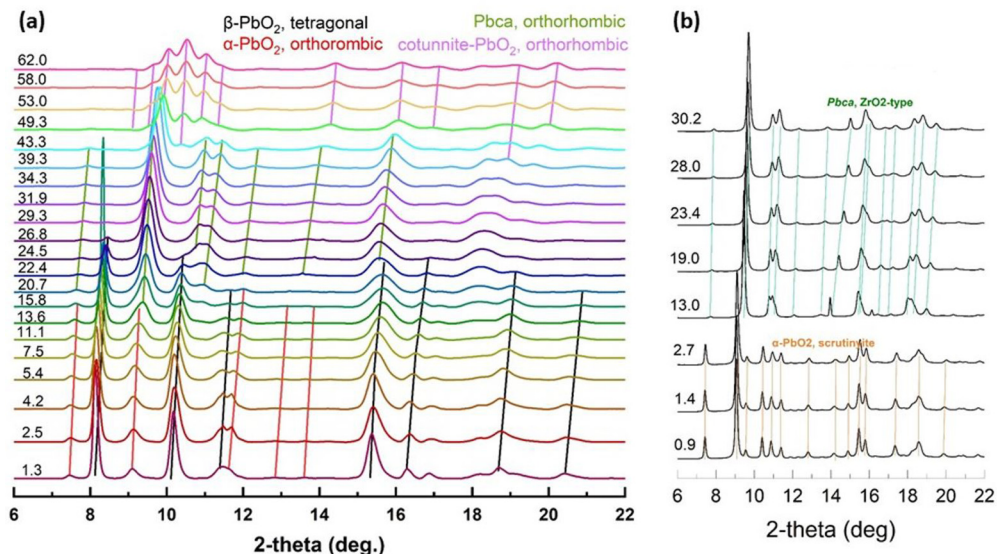


FIG. 2. X-ray diffraction patterns collected at room temperature during (a) compression and (b) decompression of PbO₂. Solid lines follow the peak positions of relevant phases. Pressure values are listed to the left of each pattern.

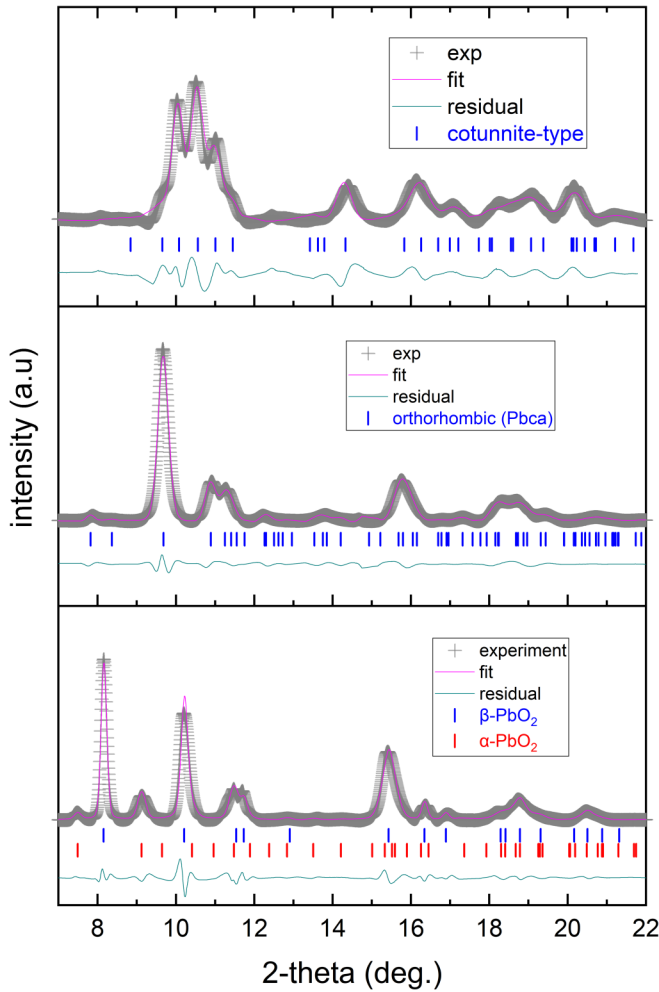


FIG. 3. Room temperature x-ray diffraction patterns (crosses) collected at 2.5 GPa (bottom), 34.3 GPa (medium) and 58 GPa (top) and corresponding Rietveld refinement (red curve).

can be indexed to the cotunnite-type orthorhombic structure (space group $Pnam$), which is also found to be stable at the highest pressure 62 GPa reached in this paper. Decompression from the ZrO_2 -type $Pbca$ phase produces a pure α - PbO_2 ($Pbcn$) scrutinyite phase, with no evidence of any material reverting to the starting-phase β - PbO_2 rutile structure [Figure 2(b)]. These results are generally in good agreement with previous findings (Grocholski *et al.* [4]) and document common behavior for all group-IV oxides that are compressed to phases with greater density than the rutile-type structure.

Examples of diffraction patterns from $Pbca$ and $Pnam$ orthorhombic phases obtained on compression to 34.3 and 58 GPa, respectively, are depicted in Fig. 3. The corresponding volume changes from 2.5 to 34.3 and to 58 GPa are in turn 19.7(4) and 30.3(3)%, with cell constants obtained from structure refinements: $a = b = 4.9327(7)$ Å, $c = 3.3743(8)$ Å, and $a = 4.9583(18)$ Å, $b = 5.8945(31)$ Å, $c = 5.4692(28)$ Å for β - PbO_2 and α - PbO_2 , respectively. At 34.3 GPa, the refined cell constants are $a = 10.1205(37)$ Å, $b = 5.2253(8)$ Å, and $c = 4.9848(15)$ Å for the $Pbca$ orthorhombic structure. The axial ratios a/c and b/c of the cotunnite structure are 1.6258(8) and 1.9403(9) at 58 GPa. These results show good agreement

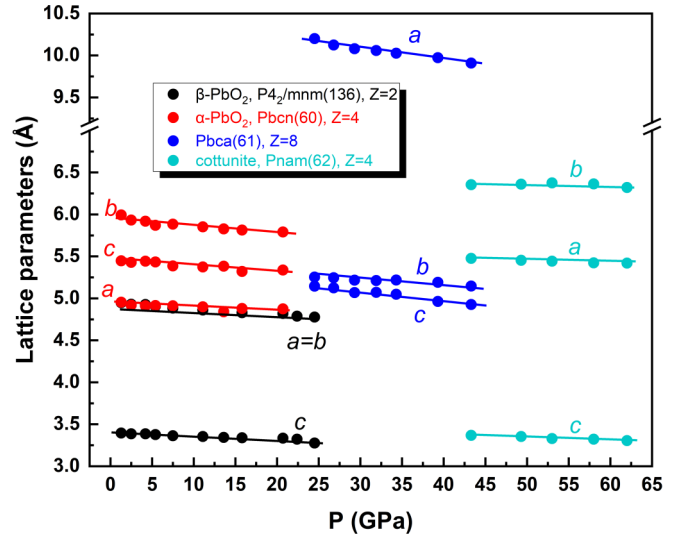


FIG. 4. Lattice parameters measured on compression at room temperature. Solid lines are least squares fits.

with those of cotunnite-type ZrO_2 and HfO_2 : a/c , $b/c = 1.678$, 1.945, and 1.676, 1.951, respectively [36].

At 24.5 GPa, the refined cell constants are $a = 10.2011(49)$ Å, $b = 5.2540(15)$ Å, and $c = 5.1450(16)$ Å for the orthorhombic phase with space group $Pbca$, which are comparable with ZrO_2 orthorhombic phases under ambient conditions (Fig. 4) [37]. Due to the similarities between lattice parameters, a structural model based on $Pbca$ was applied to the data collected in the pressure range 24.5–43.3 GPa, and these refinements yield good fits to the experimental profile $R_{Bragg} = 8.1\%$. From the variation of molar volume (V/Z) of PbO_2 phases with pressure, two structural transitions occur ~ 24 and ~ 43 GPa, accompanied by unit-cell volume changes of ~ 7.8 and $\sim 6.7\%$ (Fig. 5). We do not find the

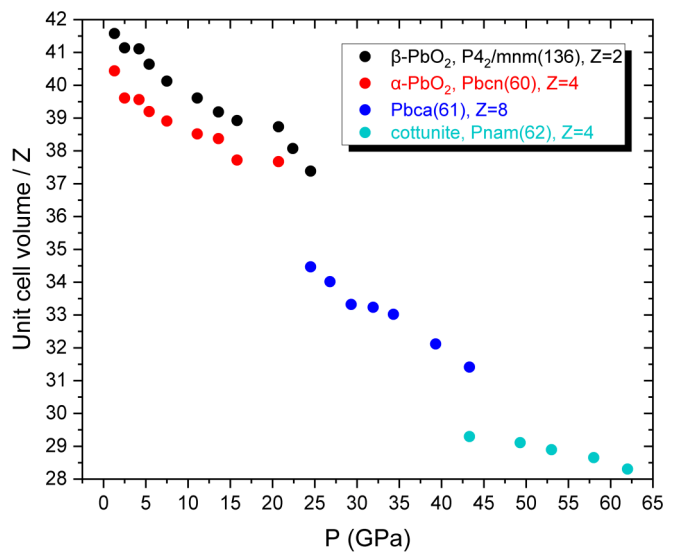


FIG. 5. Measured unit-cell volumes for β - PbO_2 ($Z = 2$), α - PbO_2 ($Z = 4$), and orthorhombic $Pbca$ ($Z = 8$) and $Pnam$ ($Z = 4$) phases on compression at room temperature. Uncertainties are smaller than the symbol sizes. Solid lines are least squares fits.

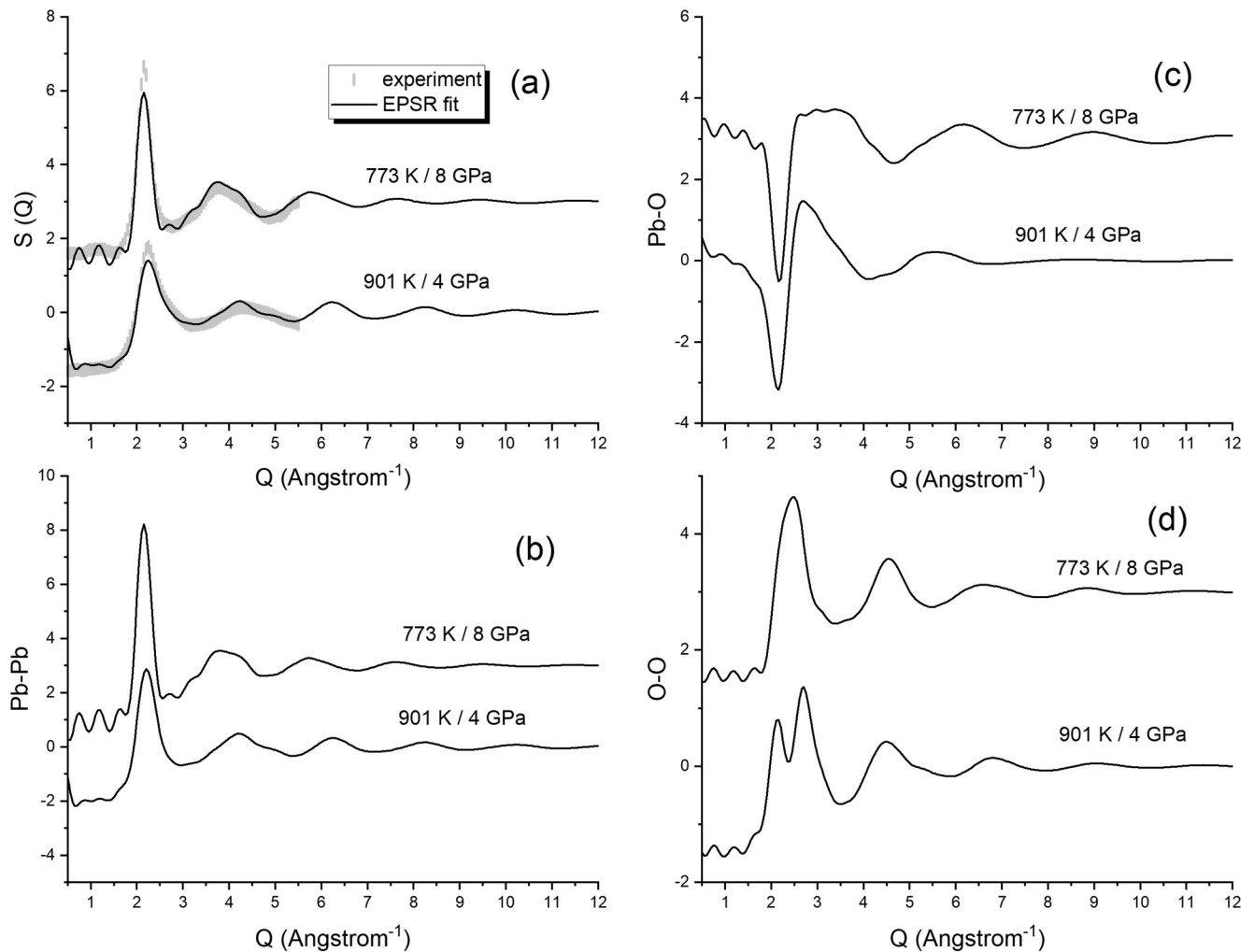


FIG. 6. (a) Total structure factors $S(Q)$ at 901 K and 4 GPa (bottom curves) and at 773 K and 8 GPa (top curves). Partial structure factors for (b) Pb-Pb, (c) Pb-O, and (d) O-O pairs calculated from empirical potential structure refinement (EPSR) simulations.

baddeleyite-type structure in room-temperature compression measurements, as reported by Grocholski *et al.* [4]. The phase-transition sequence with increasing pressure is mixed phase (α - $\text{PbO}_2 + \beta$ - PbO_2) \rightarrow $Pbca$ \rightarrow cotunnite phase. In this paper, we thus find the pure stable cotunnite phase without laser heating, in contrast with the results of Grocholski *et al.* [4] and Haines and Leger [19], who observed the cotunnite phase mixed with $Pbca$ between 29 and 47 GPa. As discussed below, the apparent disparities in observations can be attributed to differences in shear stresses present in each experiment.

B. Melt- PbO_2 under pressure

The structural evolution of liquid PbO_2 was studied using high-pressure–high-temperature *in situ* diffraction. Melt phases were obtained at 901 K and 4 GPa and at 773 K and 8 GPa, indicating a crystal-liquid phase boundary with a negative P - T slope, $dP/dT = -0.031 \text{ GPa K}^{-1}$. Since the entropy upon melting is positive, the negative slope implies that liquid PbO_2 is denser than the parent crystal PbO_2 . Figure 6(a) shows our experimental structure-factor [$S(Q)$] patterns and

corresponding EPSR simulations, with PSFs for Pb-Pb, Pb-O, and O-O pairs, obtained from these simulations, shown in Figs. 6(b)–6(d). The small differences visible at low- Q values in $S(Q)$ are mostly due to the finite box size used in the simulations. The main experimental $S(Q)$ peaks are found to be a little more intense than that of simulated counterparts. This could arise from imperfect normalization of $S(Q)$ due to the limited Q range used. It is difficult to mark the center of the second $S(Q)$ peaks since these peaks are broad, and the intensity of these broad peaks is not large enough to make an accurate identification. All the peaks in the $S(Q)$ of the data collected at 901 K/4 GPa are located at higher Q values than its counterpart at 773 K/8 GPa, which indicates a denser melt PbO_2 at lower P and higher T . Reduction of the raw scattering data to structure factors and derivation of PSFs by direct inversion of the total $S(Q)$ are described in Refs. [38,39]. Simulated PSFs indicate that the most dominant contribution to the principal peak located at 2.1 \AA^{-1} in the $S(Q)$ comes from Pb-Pb (dominant) and O-O correlations; Pb-O anticorrelations cause a partial cancellation of the principal peak. The principal peak of $S(Q)$ at 773 K and 8 GPa is more intense than that at 901 K and 4 GPa, suggesting more

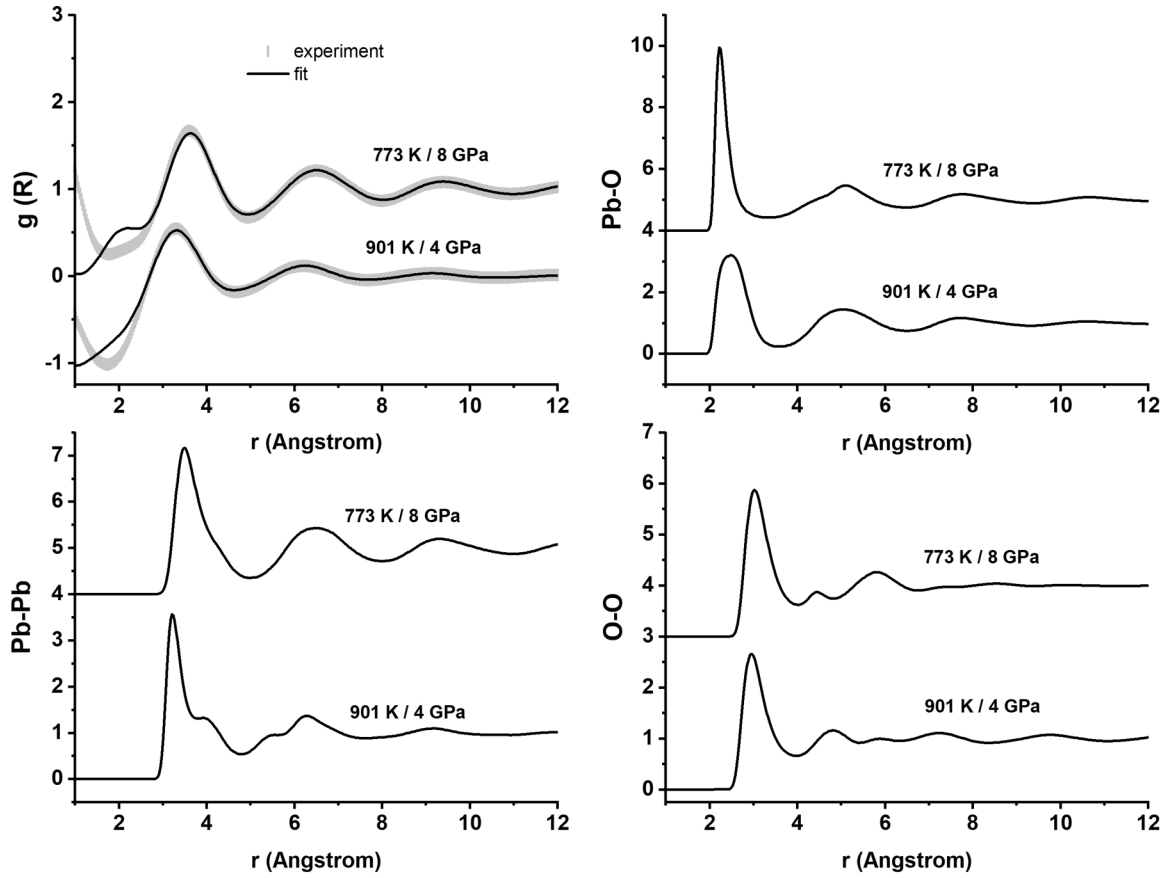


FIG. 7. Experimental and simulated radial distribution functions (RDFs) at 901 K/4 GPa (bottom curves) and 773 K/8 GPa (top curves) and corresponding Pb-Pb, Pb-O, and O-O pair distribution functions calculated from the empirical potential structure refinement (EPSR) simulations.

short-range structural order at a length scale of ~ 2.9 Å manifested by Pb-Pb and O-O correlations. The most prominent peak in the O-O PSF for the 4 GPa data has a clear shoulder on the low- Q side, which is distinct from the results at 8 GPa that show a broad peak in the $Q = 1.8\text{--}3.4$ Å $^{-1}$ range attributable to overlapping of the prominent peak and shoulder.

Structural analysis in real space was conducted using the experimental and simulated RDFs, as summarized in Fig. 7. The RDFs at the two pressure-temperature conditions [Fig. 7(a)] are not significantly different from each other in terms of their shapes, except for the peak positions. The corresponding Pb-Pb, Pb-O, and O-O pair distribution functions [Figs. 7(b)–7(d)] determined from EPSR simulations indicate that all nearest-neighbor correlations contribute to the first peak in the RDFs. The Pb-Pb, Pb-O, and O-O nearest-neighbor distances are calculated to be in the ranges of 3.2–3.5, 2.2–2.5, and 2.9–3.1 Å (first peaks in relevant partial RDFs and the nearest-neighbor distance in $g(r)$) are listed in

Table II for the melt phases obtained at 901 K and 4 GPa and at 773 K and 8 GPa). The first $g(r)$ peak and the Pb-Pb and O-O bond lengths of melt PbO₂ are found at shorter distances at 901 K and 4 GPa than that of 773 K and 8 GPa data. This suggests that melt PbO₂ at 901 K and 4 GPa is less dense than its counterpart at 773 K and 8 GPa, which is also in agreement with the negative P - T slope.

The broadening observed for the first Pb-O peak at 4 GPa data is attributed to a range of coordination numbers being present around Pb. Nearest-neighbor O-coordination numbers around Pb atoms n_{PbO} obtained by integrating the area of the corresponding peak in the Pb-O PDF are 7.8(7) and 8.7(6) for 4 and 8 GPa, respectively. This trend shows that, with rising pressure, the coordination number of oxygen around lead in the melt gradually increases to $n_{\text{PbO}} \approx 9\text{--}10$. This reflects the 4- to 5-coordination of Pb around O with rising pressure, consistent with the calculated n_{OPb} values that increase from 3.8(4) at 4 GPa to 4.3(4) at 8 GPa.

TABLE II. The bond lengths of Pb-Pb, Pb-O, and O-O in melt PbO₂.

P (GPa)	T (K)	First peak in $g(r)$ (Å)	Pb-Pb (Å)	Pb-O (Å)	O-O (Å)
8	773	3.596	3.493	2.237	3.029
4	901	3.293	3.219	2.452	2.956

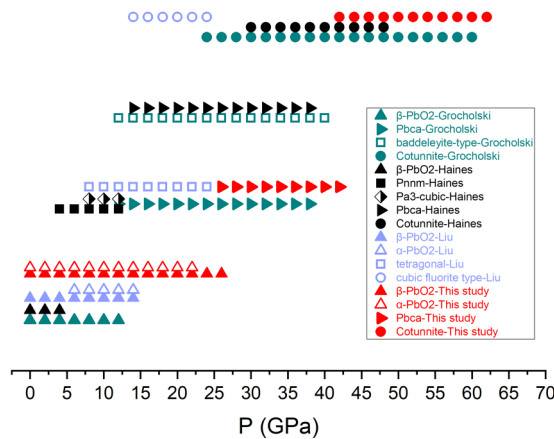


FIG. 8. Summary of compression results obtained in this paper alongside the phase transitions reported for PbO_2 by Liu [40], Haines *et al.* [36] and Grocholski *et al.* [4].

C. Discussion

Figure 8 summarizes our results in comparison with the phase transitions reported for PbO_2 by Liu [40], Haines *et al.* [36], and Grocholski *et al.* [4]. A comparison of the onset pressures for the phase transitions from the starting phase to orthorhombic ($Pbca$) and for the formation of the high-pressure cotunnite-type structure indicates that all transitions start at significantly higher pressures in our case as compared with those reported by Haines *et al.* [36] and Grocholski *et al.* [4]. These differences lead us to conclude that the pressure transmitting medium is a key factor affecting the pressure-induced transformations of PbO_2 , with shear stresses (i.e., nonhydrostatic conditions) and resulting defects helping to overcome kinetic barriers to transformation.

Specifically, we used Ne, whereas Haines *et al.* [36] and Grocholski *et al.* [4] used silicone grease and Ar as pressure media, respectively, which provide less hydrostatic conditions than Ne. The difference between Ne and Ar is related to the difference in their atomic radii, Ne (0.38 Å) and Ar (0.71 Å), and consequently, Ar shows a low solidification pressure ~ 1.4 GPa at room temperature (4.8 GPa for Ne) and a hydrostatic limit of ~ 9 GPa (~ 15 GPa for Ne). Silicone grease supports even larger deviatoric stresses than noble gases and therefore causes the appearance of phase transitions at lower pressures.

Moreover, Grocholski *et al.* [4] and Haines *et al.* [36] and report that the cotunnite-type structure ($Pnam$) was found coexisting with the orthorhombic ($Pbca$) and baddeleyite structures in the pressure ranges ~ 22 – 40 and ~ 30 – 40 GPa, respectively. Liu [40] reported the cubic fluorite-type structure as the high-pressure phase in the range of 12 – 22 GPa, coexisting with the tetragonal form. Our results do not show any phase coexistence $> \sim 25$ GPa, and this is attributed to the

largely hydrostatic conditions in this paper, i.e., the absence of significant shear stress or strain in the sample chamber, making the $(\beta\text{-PbO}_2 + \alpha\text{-PbO}_2) \rightarrow Pbca \rightarrow$ cotunnite-type structure transition pathway favorable in this paper.

The cotunnite structure consisting of ninefold coordinated cations is the expected structure of silica in the multi-Mbar regime. Therefore, this leads us to consider melt PbO_2 as an important analog for liquid metallic silicates at the extreme conditions relevant to the interiors of large planets. Our results obtained from molten PbO_2 provide evidence for highly coordinated Pb cations, with the first-neighbor coordination of O around Pb increasing from $\sim 7.8(7)$ to $8.7(6)$ between 4 and 8 GPa.

IV. CONCLUSIONS

Up to 65 GPa, PbO_2 is found to undergo two transitions at room temperature, beginning with a mixture of rutile and orthorhombic structures and ending with the cotunnite structure. The first transition is to a $Pbca$ phase, observed at ~ 22 GPa, with a further transition to the cotunnite phase at ~ 43 GPa corresponding to a change in coordination number around Pb atoms from 6 to 7 and to 9, respectively. We find the pure cotunnite phase without laser heating. The ZrO_2 -type $Pbca$ phase transforms to $\alpha\text{-PbO}_2$ ($Pbcn$) scrutinyite phase upon decompression < 13 GPa, and this is retained down close to ambient pressure. Compared with previous studies reported by Haines *et al.* [36] and Grocholski *et al.* [4], all transitions observed in this paper start at significantly higher pressures, indicating that the pressure-transmitting medium influences the transformation kinetics and perhaps the phase stability via the amount of deviatoric stress and strain that are present. The distribution of coordination numbers in melt PbO_2 , obtained by empirical potential structure refinements of x-ray diffraction patterns, suggest the range of liquid metallic silicate structures achieved at extreme planetary conditions.

ACKNOWLEDGMENTS

This research used resources of the Advanced Light Source, a U.S. DOE Office of Science User Facility under contract no. DE-AC02-05CH11231, and was partially supported by COMPRES, the Consortium for Materials Properties Research in Earth Sciences under NSF Cooperative Agreement EAR 1606856. B.K.G. acknowledges help provided by T. J. Smart in the procurement of the sample and initial help with the experiment. We are also thankful for support from the National Nuclear Security Administration (NNSA) through the Center for Matters under Extreme Pressure (CMEC) at University of California San Diego (UCSD) and from NSF through Center of Matter at Atomic Pressures (CMAP) at University of Rochester.

[1] M. Millot, N. Dubrovinskaia, A. Cernok, S. Blaha, L. Dubrovinsky, D. G. Braun, P. M. Celliers, G. W. Collins, J. H. Eggert, and R. Jeanloz, Shock compression of stishovite and melting of silica at planetary interior conditions, *Science* **347**, 418 (2015).

[2] V. P. Prakapenka, G. Shen, L. S. Dubrovinsky, M. L. Rivers, and S. R. Sutton, High pressure induced phase transformation of SiO_2 and GeO_2 : Difference and similarity, *J. Phys. Chem. Solids* **65**, 1537 (2004).

- [3] Y. Kuwayama, K. Hirose, N. Sata, and Y. Ohishi, The pyrite-type high pressure form of silica, *Science* **309**, 923 (2005).
- [4] B. Grocholski, S.-H. Shim, E. Cottrell, and V. B. Prakapenka, Crystal structure and compressibility of lead oxide up to 140 GPa, *Am. Mineral.* **99**, 170 (2014).
- [5] A. R. Oganov, M. J. Gillan, and G. D. Price, Structural stability of silica at high pressures and temperatures, *Phys. Rev. B* **71**, 064104 (2005).
- [6] K. Umemoto, R. Wentzcovitch, and P. B. Allen, Dissociation of MgSiO_3 in cores of gas giants and terrestrial exoplanets, *Science* **311**, 983 (2006).
- [7] T. Tsuchiya and J. Tsuchiya, Prediction of a hexagonal SiO_2 phase affecting stabilities of MgSiO_3 and CaSiO_3 at multi-megabar pressures, *Proc. Natl. Acad. Sci. USA* **108**, 1252 (2011).
- [8] S. Wu, K. Umemoto, M. Ji, C.-Z. Wang, K.-M. Ho, and R. M. Wentzcovitch, Identification of post-pyrite phase transitions in SiO_2 by a genetic algorithm, *Phys. Rev. B* **83**, 184102 (2011).
- [9] Y. Usui and T. Tsuchiya, Ab initio two phase molecular dynamics on the melting curve of SiO_2 , *J. Earth Sci.* **21**, 801 (2010).
- [10] M. J. Lyle, C. J. Pickard, and R. J. Needs, Prediction of 10-fold coordinated TiO_2 and SiO_2 structures at multi-megabar pressures, *Proc. Natl. Acad. Sci. USA* **112**, 6898 (2015).
- [11] Y. Al-Khatatbeh, B. Kiefer, and K. M. Lee, High-pressure behavior of TiO_2 as determined by experiment and theory, *Phys. Rev. B* **79**, 134114 (2009).
- [12] N. A. Dubrovinskaya, L. Dubrovinsky, R. Ahuja, V. B. Prokopenko, V. Dmitriev, H.-P. Weber, J. M. Osorio-Guillen, and B. Johansson, Experimental and Theoretical Identification of a New High-Pressure TiO_2 Polymorph, *Phys. Rev. Lett.* **87**, 275501 (2001).
- [13] H. Dekura, T. Tsuchiya, Y. Kuwayama, and J. Tsuchiya, Theoretical and Experimental Evidence for a New Post-Cotunnite Phase of Titanium Dioxide with Significant Optical Absorption, *Phys. Rev. Lett.* **107**, 045701 (2011).
- [14] X. Zhong, J. Wang, S. Zhnag, G. Yang, and Y. Wang, Ten-fold coordinated polymorph and metallization of TiO_2 under high pressure, *RSC Adv.* **5**, 54253 (2015).
- [15] J. P. Itie, A. Polian, and J. M. Besson, Optical-absorption edge of CsI up to 58 GPa, *Phys. Rev. B* **30**, 2309 (1984).
- [16] J. Haines, J. M. Leger, and C. Chateau, Transition to a crystalline high pressure phase in $\alpha\text{-GeO}_2$ at room temperature, *Phys. Rev. B* **61**, 8701 (2000).
- [17] S. Ono, T. Tsuchiya, K. Hirose, and Y. Ohishi, High-pressure form of pyrite-type germanium dioxide, *Phys. Rev. B* **68**, 014103 (2003).
- [18] Z. Lodziana, K. Parlinski, and J. Hafner, Ab initio studies of high-pressure transformations in GeO_2 , *Phys. Rev. B* **63**, 134106 (2001).
- [19] J. Haines and J. M. Leger, X-ray diffraction study of the phase transitions and structural evolution of tin dioxide at high pressure: relationships between structure types and implications for other rutile-type dioxides, *Phys. Rev. B* **55**, 11144 (1997).
- [20] S. Ono, K. Funakoshi, A. Nozawa, and T. Kikegawa, High-pressure phase transitions in SnO_2 , *J. Appl. Phys.* **97**, 073523 (2005).
- [21] S. R. Shieh, A. Kubo, and T. S. Duffy, High pressure phases in SnO_2 to 117 Gpa, *Phys. Rev. B* **73**, 014105 (2006).
- [22] E. A. Petigura, A. W. Howard, and G. W. Marcy, Prevalence of Earth-size planets orbiting sun like stars, *Proc. Natl. Acad. Sci. USA* **110**, 19273 (2013).
- [23] S. Mazevet, T. Tsuchiya, A. Benuzzi-Mounaix, and F. Guyot, Melting and metallization of silica in the cores of gas giants, ice giants, and super Earths, *Phys. Rev. B* **92**, 014105 (2015).
- [24] H. K. Mao, J. Xu, and P. M. Bell, Calibration of the ruby pressure gauge to 800 kbar under quasi-hydrostatic conditions, *J. Geophys. Res.* **91**, 4673 (1986).
- [25] S. V. Raju, J. M. Zaug, B. Chen, J. Yan, J. Knight, R. Jeanloz, and S. M. Clark, Determination of the variation of the fluorescence line positions of the ruby, strontium tetraborate, alexandrite and strontium-doped ytterbium aluminum garnet with pressure and temperature, *J. Appl. Phys.* **110**, 023521 (2011).
- [26] M. Kunz, A. A. MacDowell, A. W. Caldwell, D. Cambie, R. S. Celestre, E. E. Domning, R. M. Duarte, A. E. Gleason, J. M. Glossinger, N. Kelez, D. W. Plate, T. Yu, J. M. Zaug, H. Padmore, R. Jeanloz, P. Alivisatos, and S. M. Clark, A beamline for high pressure studies at the Advanced Light Source with a superconducting bending magnet as the source, *J. Synchrotron Rad.* **12**, 650 (2005).
- [27] A. P. Hammersley, FIT2D: A multipurpose data reduction, analysis and visualization program, *J. Appl. Cryst.* **49**, 646 (2016).
- [28] C. Prescher and V. B. Prakapenka, DIOPTAS: A program for reduction of two-dimensional x-ray diffraction data and data exploration, *High Press. Res.* **35**, 223 (2015).
- [29] Basic demonstration of CELREF unit-cell refinement software on a multiphase system, <http://mill2.chem.ucl.ac.uk/tutorial/lmgp/celref.htm>.
- [30] A. C. Larson and R. B. Von Dreele, General Structure Analysis System (GSAS), Los Alamos National Laboratory Report LAUR 86-748 (2004).
- [31] A. K. Soper, On the uniqueness of structure extracted from diffraction experiments on liquids and glasses, *J. Phys.: Condens. Matter* **19**, 415108 (2007).
- [32] A. K. Soper, Empirical potential Monte Carlo simulations of fluid structure, *Chem. Phys.* **202**, 295 (1996).
- [33] O. L. G. Alderman, A. C. Hannon, D. Holland, S. Feller, G. Lehr, A. J. Vitale, U. Hoppe, M. v Zimmermann, and A. Watenphul, Lone-pair distribution and plumbite network formation in high lead silicate glass, $80\text{PbO} \cdot 20\text{SiO}_2$, *Phys. Chem. Chem. Phys.* **15**, 8506 (2013).
- [34] C. Y. Maghfiroh, A. Arkundato, Misto, and W. Maulina, Parameters (σ , ϵ) of Lennard-Jones for Fe, Ni, Pb for potential and Cr based on melting point values using the molecular dynamics method of the LAMMPS program, *J. Phys.: Conf. Ser.* **1491**, 012022 (2020).
- [35] W. B. White, F. Dacheville, and R. Roy, High-pressure-high-temperature polymorphism of the oxides of lead, *J. Am. Ceram. Soc.* **44**, 170 (1961).
- [36] J. Haines, J. M. Leger, and O. Schulte, The high pressure phase transition sequence from the rutile-type through to the cotunnite-type structure in PbO_2 , *J. Phys.: Condens. Matter* **8**, 1631 (1996).
- [37] O. Ohtaka, T. Yamanaka, S. Kume, N. Hara, H. Asano, and F. Izumi, Structural analysis of orthorhombic ZrO_2 by high

- resolution neutron powder diffraction, *Proc. Jpn. Acad. B* **66**, 193 (1990).
- [38] B. Kalkan, B. Godwal, S. V. Raju, and R. Jeanloz, Local structure of molten AuGa₂ under pressure: Evidence for coordination change and planetary implications, *Sci. Rep.* **8**, 6844 (2018).
- [39] A. K. Soper, Partial structure factors from disordered materials diffraction data: an approach using empirical potential structure refinement, *Phys. Rev. B* **72**, 104204 (2005).
- [40] L. Liu, The high-pressure phase transformations of PbO₂: An *in-situ* x-ray diffraction study, *Phys. Chem. Minerals* **6**, 187 (1980).